The Eurasia Proceedings of Science, Technology, Engineering & Mathematics (EPSTEM)
ISSN: 2602-3199

The Eurasia Proceedings of Science, Technology, Engineering and Mathematics (EPSTEM), 2025

Volume 37, Pages 255-271

ICEAT 2025: International Conference on Engineering and Advanced Technology

Numerical Investigation of Thermal - Hydraulic Performance of a Solar Air Heater Duct with Transverse W-Shaped Rib Turbulators

Kadhim Al-Chlaihawi
University of Al-Qadisiyah

Sarah Ahed Mohammed Al-Hasnawi
Al-Furat Al-Awsat Technical University

Ahmed Kadhim Zarzoor
University of Al-Qadisiyah

Abstract: One of the effective methods that can be employed to enhance the performance of the solar thermal air heater is texturing of the absorber surface using the rib roughness. The alteration facilitates the heat transfer by the generation of turbulence and surface area increases. To analyze the thermal performance of an optimized surface roughness solar-powered air heater, the article provides a 2D numerical model of an air heater. A solar air heater (SAH) duct with W-shaped transverse ribs on an absorber plate made of two opposing right-triangular ribs are studied in this current work concerning the thermo-fluid behavior. Notable results are the Nusselt number (Nu), the friction factor (f), the thermo-hydraulic performance parameter (THPP) and distributions of fluid properties. In the computational analysis, various roughness and flow conditions are investigated, i.e. the Reynolds number (Re =6,000-18,000), non-dimensional pitch (P/e =7.14-17.86) with non-dimensional height (e/D =0.042) remaining constant. The optimum value of THPP was achieved with the suggested rib arrangement at P/e=10.71 and Re=6000. The ribbed surface has significant improvements in thermal performance, where the values of Nu have improved by 228% of smooth ducts. However, this enhancement is coupled with increased hydraulic resistance especially in the region of P/e=7.14 and Re=18,000 where the friction factor rises to 4.18 times the amount of smooth ducts.

Keywords: SAH, Thermal performance, W-shaped ribs, Collector plate, Nu

Introduction

Solar air heaters (SAHs) are based on the concept of absorbing solar radiation and convert it to heat for heating rooms, regenerate humidifying elements, and dry industrial or agricultural crops. Their performance is, however, discouraged by the development of a laminar sublayer of air over the absorbance plate (Alrashidi et al., 2024). To induce turbulence, artificial roughness is generally placed on the surface of the absorber material and breaks the layer. Although this increases the convective heat transfer, pumping power increases (Abbas Alhilali et al., 2025; Roy et al., 2024). Studies have concentrated on developing duct and roughness parameters so as to produce the best heat transfer requirements using minimum incremental pump energy.

Various approaches have been implemented in broad literature research to enhance the performance of SAHs, such as incorporating artificial roughness features, such as ribs (Kumar et al., 2014), fins (Sahu et al., 2019), baffles (Olfian et al., 2020), and winglets (Chamoli et al., 2018) into the absorbent surface of the conventional flat-plate SAHs and also impingement jets (Saini & Yadav, 2020).

- Selection and peer-review under responsibility of the Organizing Committee of the Conference

Prasad and Mullick (1983) firstly introduced the protruding wire application to enhance heat transfer in SAHs in drying cereal grains. Gupta et al. (1993) followed up by examining the thermal efficiency and fluid flow behavior of a rectangular SAH duct with transverse wire ribs attached under the absorber plate. In a rectangular duct with ribs of rectangular cross-section, Karwa (2003) carried out an experimental study on the behavior of a duct and experimented with various configurations, including transverse, inclined, continuous V-shaped, or discrete V-shaped configurations. A study by Layek et al. (2009), which was an experimental investigation on transverse chamfered rib-groove roughness in SAH ducts, showed that the maximum Nu was achieved at 18o chamfer angle, and there was progressive improvement in the value of friction factor with an increase in the chamfer angle.

The CFD analysis has transformed performance assessment of SAH, as costly and time consuming experimental techniques have been substituted by quick and inexpensive numerical analysis of the thermal and flow properties of the SAH (Bhagoria & Yadav, 2013b). Bhagoria and Yadav (2013a, 2014a, 2014b, 2014c) involved the analysis of various transverse rib arrangements in order to optimize surface roughness functions in solar air heaters using a systematic approach with 2D CFD modeling. Their analysis of equilateral triangular rib profiles revealed peak thermal hydraulic performance (THP = 2.11) occurring at specific geometric ratios of $e/D = 0.042$ and $P/e = 7.14$.

Numerical simulations by Gawande et al. (2016b) demonstrated that reverse L-shaped ribs in SAHs achieve peak thermal performance (TPF = 1.9) when configured with a $P/e = 7.14$ and $Re = 15{,}000$. Extending their previous work, Gawande et al. (2016a) compared various chamfered square rib geometries, finding the 20° chamfer angle with P/e=7.14 combination yielded superior performance (TPF=2.047) among tested configurations (0°-40° angles, P/e=7.14-17.86 range) in their CFD study. Mahananda and Senapati (2021) investigated the thermo-fluidic features of a SAH employing quarter-circular ribs. Their analysis revealed peak thermal enhancement (1.88 times), and friction penalty (3.4355 times) of smooth duct at P/e=7.14 for Reynolds numbers of 15,000 and 3,800 respectively. Rautela et al. (2023) compared B- and D-shaped roughness geometries, finding that while D-shapes produced greater Nu enhancement (21.91 times vs 2.264 times of smooth duct at Re=20,000, P/e=11.111), B-shapes offered better balanced performance with peak TPF of 1.47 across the turbulent flow regime.

The increase in Nu of 2.124 times with a corresponding 3.425 times increase in f of solar air heaters with transverse trapezoidal ribs were reported by Al-Chlaihawi et al. (2023). In a later study (2024), the group numerically analyzed a hybrid roughness design with trapezoidal ribs and a chamfered groove. Their parametric analysis showed that they would best perform at P/e=10.71 and e/D=0.042 with a TPF= 2.12. Sharma et al. (2021) conducted a numerical study focusing on the systematic evaluation of the overall performance of sine wave baffled SAHs. At constant e/D and P/e ratios, the study considered the effect of attack angle (α) and Reynolds number, concluding that α=30° provided the highest thermo-hydraulic performance increase (1.6 times baseline).

The recent study by Patel et al. (2020) in NACA 0040 profiles showed that the reverse NACA 0040 profile ribs had optimum THPP of 2.53 at e/D=0.065,P/e=5 with reverse profile ribs operating at Re=6000. In a later study (2021), the authors tested the differences between continuous and discrete NACA 0040 ribs and found that the Nu difference is minimal, whereas the f value is significantly lower. It had a reduced Nu and f reductions of 0.38-2.26% and 6.25-10 percent, respectively, compared with continuous ribs. Other numerical models by Sharma et al. (2024) found that novel rib geometries (C-shaped, reverse C-shaped, reverse R-shaped) are significantly more effective at improving the performance of SAH by providing 2.5-3.3 times the heat transfer improvement and 2.8-5.05 times increase in friction. C-shaped shape was of special promise with maximum TPF of 2.0078 at Re=4000.

The rigorous literature review shows that solar air heater (SAH) can have its performance increased significantly with the help of strategic surface changes. Different new geometries of ribs have proven to be effective in enhancing turbulent mixing and transfer of heat energy to the working fluid. Based on these improvements, this paper presents a new W-shaped transverse rib design - includes two opposite right-triangular ribs - to enhance thermo-hydraulic performance to a higher degree. To investigate the flow in the SAH duct with such W-shaped rib structures, the ANSYS Fluent 2023 R1 is used to perform the numerical simulation in detail. This experiment aims at defining the effect of major geometric variables - especially relative pitch (P/e) - at the conditioning of flow parameters (Reynolds number, Re) on the general thermo-hydraulic performance. The specific contour plots of turbulent intensity distribution, pressure fields and velocity profiles were also produced to give the very important insights on the basic thermo-fluid interactions involved in the system performance and enabling the effectiveness of the proposed rib geometry to be comprehensively evaluated.

CFD Investigation

Computational Domain

Figure 1(a) presents the 2D computational domain in the manner of analyzing flow and heat transfer by following a similar set-up as that of Chaube et al. (2006). According to ASHRAE 93-2003 standards (Standard) the SAH is provided as a rectangular duct with three sections: an entry (L1), a test (L2), and an exit (L3) that has length of 245 mm, 280 mm, and 115 mm respectively. The height and the width of the duct are 20 mm and 100 mm respectively, resulting in a hydraulic diameter of 0.0333 m and an aspect ratio of 5. A transition zone is added to create a complete developed flow prior to entering the test region to ensure the presence of a uniform velocity field throughout the field.

Transverse W-shaped ribs are suggested as the roughness elements in this study. Only ribs are placed below the top absorber plate and the rest of the surfaces are smooth. The rib geometry parameters (pitch and height) were chosen due to the experimental study of Bopche and Tandale (Bopche & Tandale, 2009). The rib height (e/D = 0.042) was maintained at constant (1.4 mm) to provide the correct interaction with the laminar sub-layer with minimal effects of the flow blockage.

In accordance with the study conducted by Verma and Prasad (2000), relative roughness pitch (P/e) should be over 10 to avoid negative effects of flow. At P/e<10 the roughness components are capable of hindering shear layer reattaching which leads to the reduction of the enhancement of heat transfer and the increase of pressure losses. The distance between ribs (pitch) was adjusted to a tolerance of 1025 mm (P/e ratio of 7.1417.86) in order to find the optimal efficiency. This compromise between enhanced thermal performance and low interference with flow reattachment behavior is achieved.The details of W- ribs are illustrated in Figure 1 (b). The study examines five Reynolds numbers (Re) in the turbulent flow regime ($6000 \leq Re \leq 18000$), achieved by systematically adjusting the inlet air velocity. Table 1 presents the duct geometrical parameters and variables used in this computational study.

The working fluid (air) was modeled with temperature-invariant thermo-physical properties, all calculated at the reference temperature of 300 K. The computational model treats all system components - including the duct walls, absorber plate, and surface roughness elements - as homogeneous and isotropic materials with uniform thermal and structural properties. The analysis assumes a two-dimensional, steady, incompressible, turbulent flow with fully developed conditions.

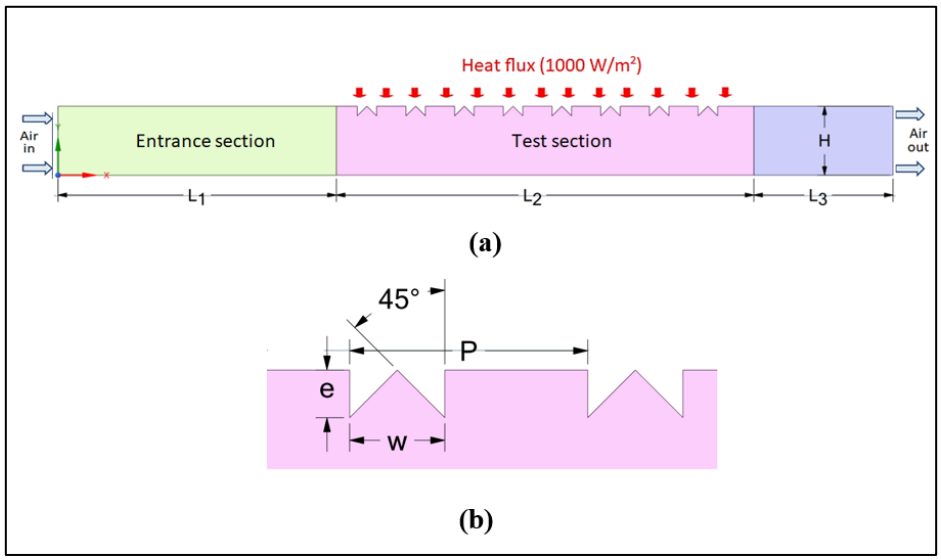

Figure 1. (a) Visual representation of the SAH including W-shaped ribbed absorber plate, and (b) detailes of W rib

Governing Equation

Based on the above mentioned assumptions, this section symmerize the governing equations as follows (Yadav & Bhagoria, 2013a):

Continuity Equation:

$$\frac{\partial(\rho u_i)}{\partial x_i} = 0\ ) \tag{1}$$

Momentum equation:

$$\frac{\partial(\rho u_i u_j)}{\partial x_i} = -\frac{\partial p}{\partial x_i} + \frac{\partial}{\partial x_i}\left[\mu\left(\frac{\partial(u_i)}{\partial x_i} + \frac{\partial(u_j)}{\partial x_i}\right)\right] + \frac{\partial\left(-\overline{\rho u_i' u_j'}\right)}{\partial x_i} \tag{2}$$

Energy equation:

$$\frac{\partial}{\partial x_i}(\rho u_i \mathrm{T}) = \frac{\partial}{\partial x_j}\left((\Gamma + \Gamma_t)\frac{\partial T}{\partial x_j}\right) \tag{3}$$

Where, Γ is the molecular thermal diffusivity and Γ_t represents its turbulent counterpart. They are identified by the following formulas (Yadav & Bhagoria, 2014b):

$$\Gamma = \frac{\mu}{Pr} \tag{4}$$

$$\Gamma_t = \frac{\mu_t}{Pr_t} \tag{5}$$

Choosing of Turbulence Model

In numerical simulations, selecting of a turbulence model is crucial as it has a direct impact on the precision of the anticipated flow and thermal properties. Figure 2 presents a comparative analysis of five widely used turbulence models by plotting the Nu against the Re for the SAH duct. The predicted Nu is also compared to known empirical correlation of smooth ducts (Eq. 13) which underscores the differences and similarities among models. The results obtained by implementing the RNG k -e model are well correlated with the results of using the Eq. (13) significant variation of less than 5%. This will ensure the accuracy of the numerical results of the existing study.

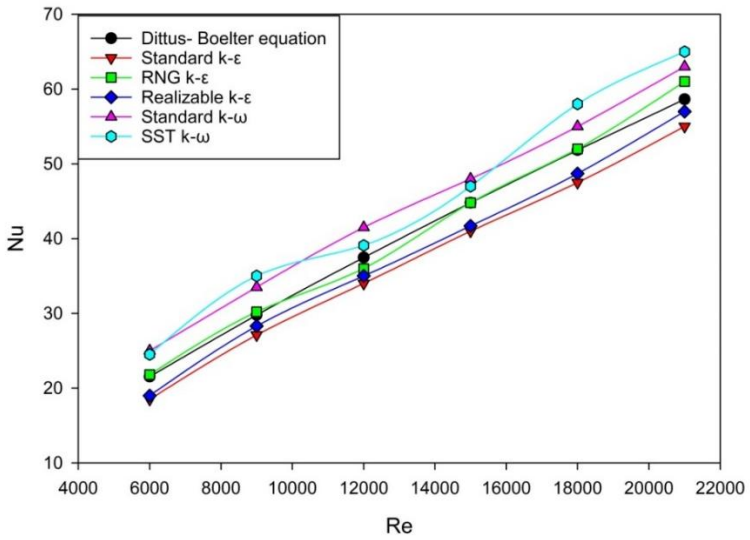

Figure 2. Plotting Nu against Re for several turbulence models

Turbulent kinetic energy (k) and dissipation rate (ε) are estimated using the following transport equations (Bhagoria & Yadav, 2013a):

$$\frac{\partial(\rho k u_i)}{\partial x_i} = \frac{\partial}{\partial x_i}\left(\alpha_k \mu_{eff}\frac{\partial k}{\partial x_i}\right) + G_k - \rho_\varepsilon \tag{6}$$

$$\frac{\partial(\rho_{\varepsilon} u_i)}{\partial x_i} = \frac{\partial}{\partial x_i}\left(\alpha_{\varepsilon}\mu_{eff}\frac{\partial \varepsilon}{\partial x_i}\right) + C_{1\varepsilon}\frac{\varepsilon}{k}(G_k) - C_{2\varepsilon}\,\rho\frac{\varepsilon^2}{k} - R_{\varepsilon} \quad) \tag{7}$$

α_k& α_{ε} both of these are referred to as inverse effective turbulence Prandtl Numbers. Also,

$$\mu_{eff} = \mu + \mu_t \tag{8}$$

$$\mu_t = \rho C_{\mu}\frac{k^2}{\varepsilon} \tag{9}$$

In the equations above, G_k represents the generation of turbulent kinetic energy due to the mean velocity gradients.This term can be expressed as

$$G_k = -\rho\acute{\mu_i}\acute{\mu_j}\frac{\partial u_j}{\partial x_i} \quad) \tag{10}$$

The RNG k-ε turbulence model employs the following empirical constants (Launder & Spalding, 1972):

$C_{1\varepsilon}$ = 1.42, $C_{2\varepsilon}$ = 1.68, C_{μ}= 0.0845, α_k = 1.39, α_{ε} = 1.39.

Important Relation

In this numerical investigation, a SAH is discussed with artificially roughened surfaces with W-shaped transverse ribs. The primary objective is to discuss how these ribs can influence Nu and f. The thermal performance of the SAH system (determined by Nu_r) should be considered as well as the hydraulic one (connected with f_r) in order to design an efficient system. The equations of calculating Nur and fr in ribbed SAH ducts are as follows:

$$\mathrm{Nu}_r = \frac{\mathrm{h\,D}}{\lambda} \quad) \tag{11}$$

$$f_r = \frac{\Delta \mathrm{P}}{2\rho \mathrm{u}^2}.\frac{\mathrm{D_h}}{\mathrm{L_2}} \quad) \tag{12}$$

The Nu_s and f_s of smooth channel may be determined using the Dittus Boelter and Blasius equations respectively (Fox et al., 1994; Kakac et al., 2013).

$$\mathrm{Nu_s} = 0.023\mathrm{Re}^{0.8}\mathrm{Pr}^{0.4} \quad) \tag{13}$$

$$f_s = 0.0791\mathrm{Re}^{-0.25} \quad) \tag{14}$$

To compare the performance of a roughened duct with that of a smooth duct run under the same pumping power, Webb and Eckert (1972) suggested a Thermal-Hydraulic Performance Parameter (THPP):

$$THPP = \frac{Nu_r/Nu_s}{\left(f_r/f\right)^{1/3}} \quad) \tag{15}$$

Optimal efficacy of the thermal performance enhancement device is observed when the THPP is exceeding unity. This dimensionless ratio is a key comparative ratio between different geometry designs to select the most efficient design numerically by performing a systematic benchmarking of the performance of different designs.

Computational Procedure

Numerical Method

Numerical calculation was done using ANSYS Fluent 2023 R1 and the space discretization was done via the Finite Volume Method (FVM). A pressure-based approach with a double-precision numerical solver was used to solve the governing equations. The convection and diffusion terms were discretized using a node based Green-Gauss method, but the momentum, energy and turbulence equations were solved using second order upwind schemes. SIMPLE algorithm was used to address the pressure-velocity coupling to get sound convergence. The accuracy of the solution was checked in terms of scaled residuals whereby continuity and momentum equations were checked with convergence criteria of 10^4 and energy equation of 10^6.

Boundary Conditions

This paper is a numerical analysis of the turbulent flow and thermal characteristics of air in a duct with a rectangular SAH with W rib turbulators. There is adiabatic downstream and upstream parts of the computational domain. The thermal boundary conditions had a uniform heat flux of 1000 W/m 2 on the plate of the absorber. The numerical model applied no-slip wall boundary conditions on all solid surfaces imposing zero relative velocity between the fluid and solid. Uniform inlet velocity of 3.02-9.07 m/s (Re = 6000-18000) were specified at the duct entrance. The incoming air stream was maintained at an isothermal condition of 300 K, while the outlet employs a pressure-based boundary condition set to atmospheric pressure (1.013×10^5 Pa).

Grid Generation

A non-uniform grid consisting of 358,084 quadrilateral cells was employed to accurately resolve the laminar sub-layer (Figure 3). To ensure grid independence, thorough testing was conducted by progressively increasing mesh density and applying various mesh grading techniques. The refinement process stopped when further changes yielded differences of less than 1% between successive results. The grid independence test evaluated seven different mesh sizes, see Table 1. The analysis carried out for P/e=10.71, and Re=15000. The analysis revealed only negligible improvements in Nu and *f* when increasing the cell count from 358,084 to 385,737. Consequently, no significant benefit was observed in using more cells beyond this point. As a result, the grid system with 358,084 cells was selected for the present computations.

Table 1. Influence of grid element on Nu and f for $P/e = 10.71$, and $Re = 12000$.

Sl. No.	Number of elements	Nu	% variation of Nu	f	% variation of f
1	80,174	91.502	---	0.027	---
2	104,139	96.959	5.629	0.027	1.398
3	142,648	103.978	6.750	0.028	1.362
4	204,977	112.212	7.338	0.028	1.631
5	319,018	118.755	5.510	0.028	0.671
6	358,084	121.173	1.995	0.028	0.607
7	385,737	121.399	0.187	0.028	0.080

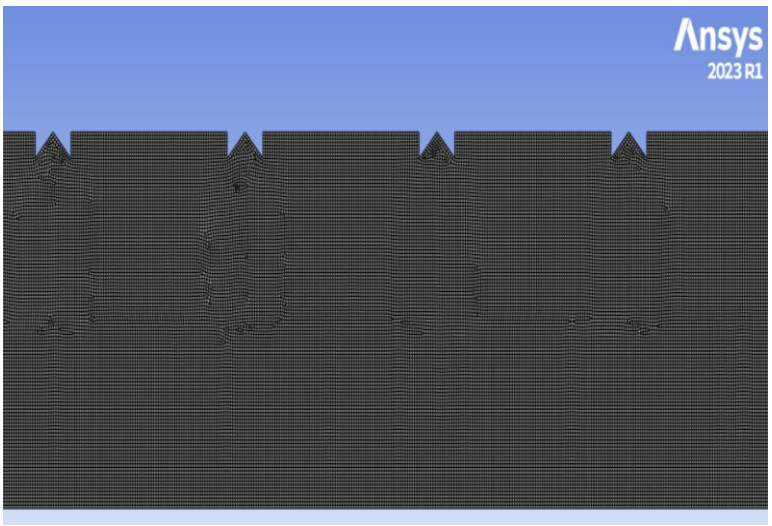

Figure 3. Grid arrangement for the computation domain.

Validation

To guarantee the accuracy of the CFD methodology, the outcomes for smooth duct are compared against both an experimental data of Gawande et al. (2016b) and the empirical correlations [Eqs. 13 and 14]. The current CFD results showed an average deviation of around 2-2.9% and 5.21-7.1% for Nu and f, respectively (Figure. 4 a and b).

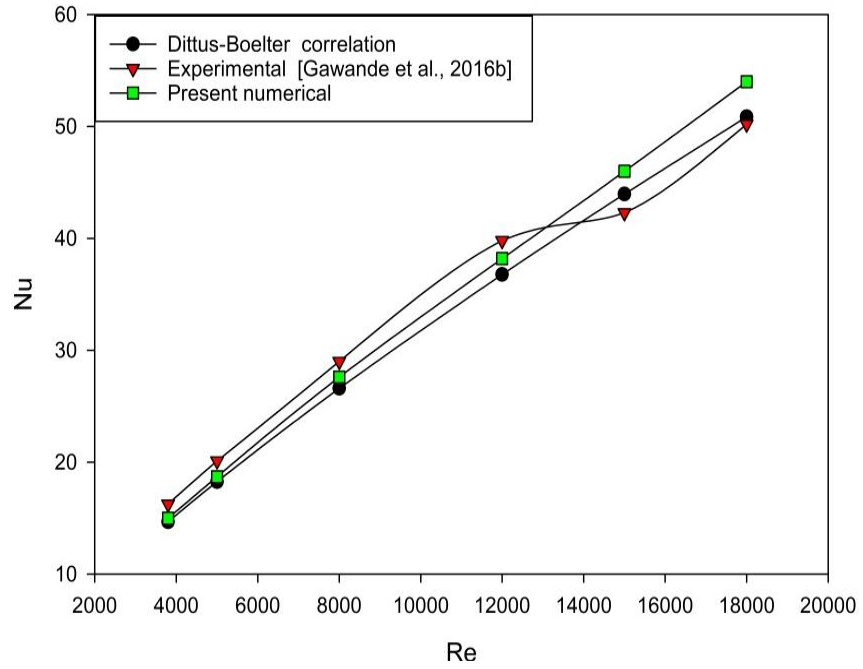

(a)

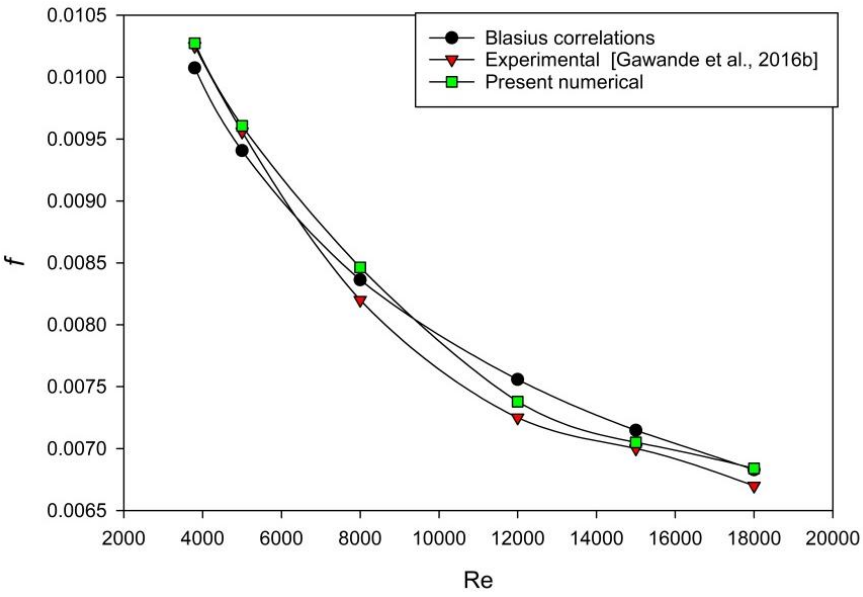

(b)

Figure 4. Comparison of (a) Nu and (b) f for the present computation with the previously published data for smooth duct

The precision of our computational approach was confirmed by comparing the computed average Nu values for the reverse-L roughened SAH with Gawande et al.'s experimental and numerical data (Gawande et al., 2016b), shown in Figure. 5. The figure clearly demonstrates that the Nu derived from the current calculation agrees with the existing experimental and numerical data in a very good manner. The current estimated Nu deviates from the

experimental and numerical values by an absolute mean of 5.2% and 3.4%, respectively. Thus, these comparisons demonstrate the acceptance of the current numerical technique.

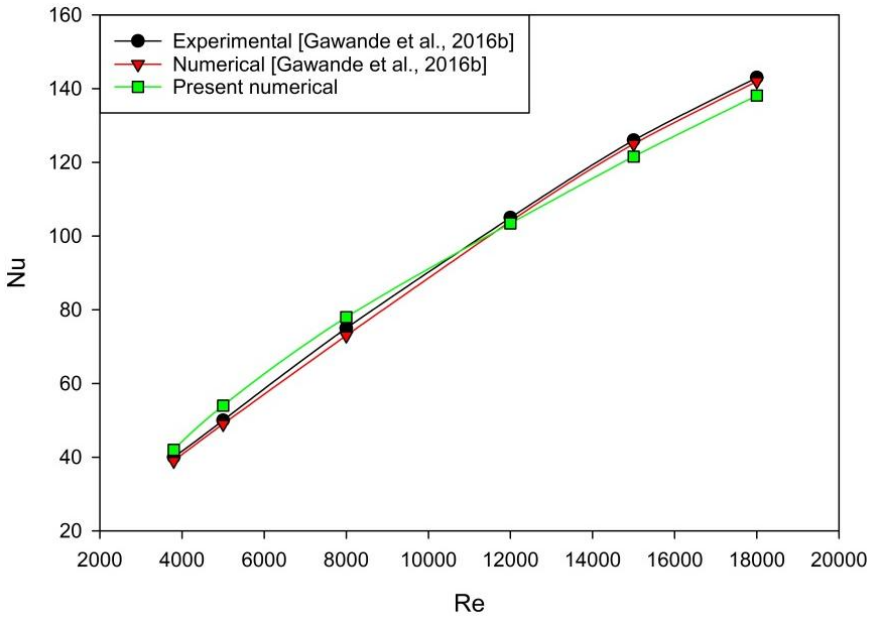

Figure 5. Comparison of Nu of current computation with available data for roughened SAH for $P/e = 10.71$ and $e/D = 0.042$.

Results and Discussion

The study numerically analyzes heat transfer and flow dynamics in a ribbed SAH duct with W-shaped transverse ribs, assessing performance via Nu, *f*, THPP, and flow field characteristics.

Heat Transfer Analysis

Employing ribs on the heated aluminum absorber plate of SAH significantly boosts heat transfer. The ribbed arrangement has a higher area of convective heat transfer as opposed to smooth surfaces, although it also adds thermal resistance, which inhibits conductive heat transfer. Also, the ribs interfere with the boundary layer in the airflow and enhance thermal performance even more.

Average Nu

The average Nu is used to estimate the heat transfer performance of the SAH when transverse W-ribbed absorber plate is used. Figure 6(a) shows the correlation of average Nu and Re at different P/e ratios. The roughness induced by the ribs changes the flow behavior of the fluid and leads to a separation of the flow, and reattachment as well as a secondary vortex. These considerations significantly increase the average Nu relative to a plain, smooth duct. The average Nu increases with an increase in Re just as it is expected. This tendency has been explained by greater kinetic energy and rate of dissipation in higher Re that enhances mixing rate and enhances heat transfer. Moreover, thermal performance is further enhanced by the fact that the increase in the thickness of the thermal boundary layer in the case of higher Re. The greater velocity of the flow facilitates turbulence and a vortex is formed on the rib surfaces and hence enhances the flow of heat between the flowing air and the absorbing plate.

To further examine the effect of P/e on the average Nu, Figure 6 (b) re-graphs the data of Figure 6(a). Although P/e does not have significant effect on Nu at lower Reynolds, at higher Reynolds, it has a significant effect as shown by the fact that NU rises first to reach a certain optimal P/e ratio (P/e = 10.71) and then it decreases. It is the highest average heat transfer efficiency. The decrease in Nu with increase in P/e value can be attributed to the fact that there are fewer points of flow reattachment on the absorber plate thereby reducing the thermal exchange.

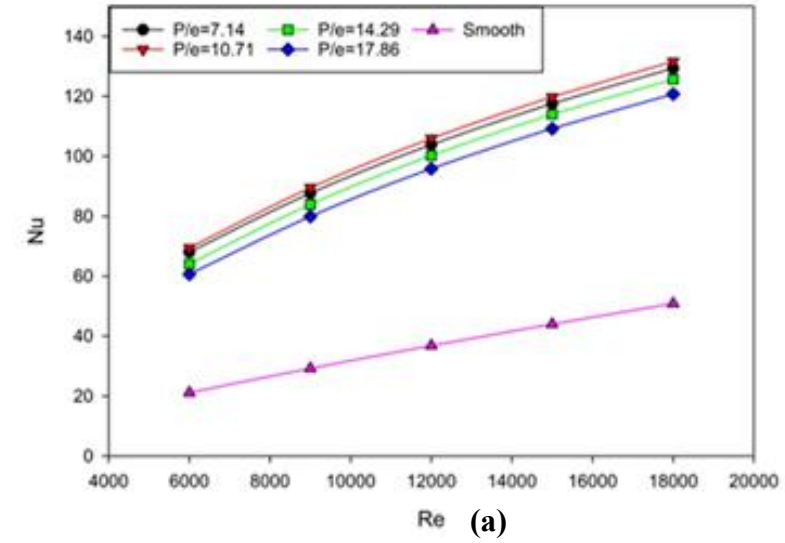

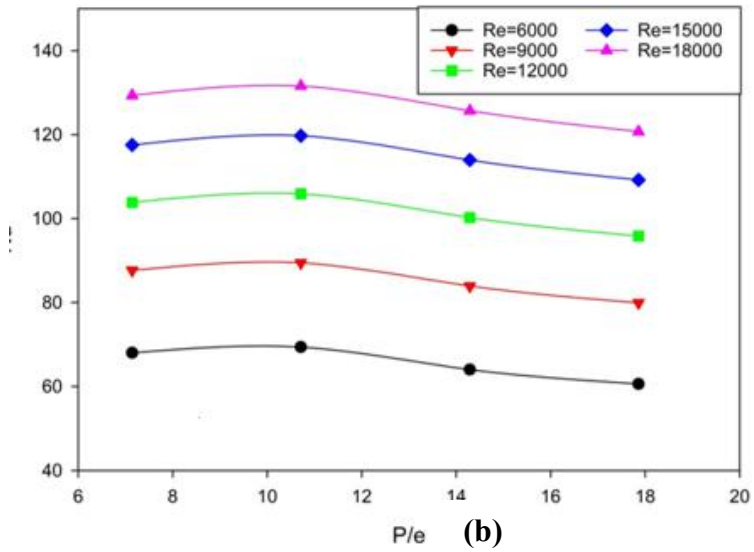

Figure 6. Average Nu verses (a) Re, (b) P/e

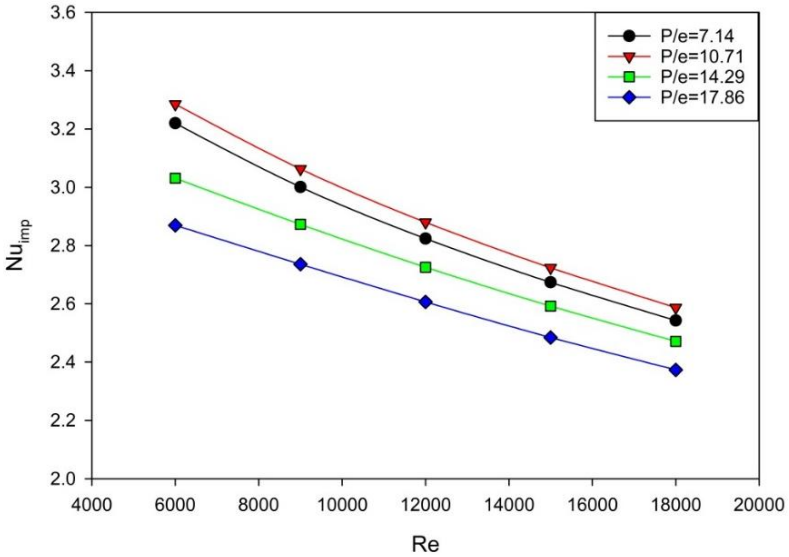

Figure 7. Nu_{imp} ratio verses Re at varying P/e values.

Figure 7 shows how the Nu improvement ratio (Nu_{imp}) varies with Re at different P/e ratios. Nu_{imp}, which is ratio of the mean Nu in a ribbed SAH to the mean Nu in a smooth duct, is exhibiting a steady decline in values as Re moves upward between 6,000 to 18,000 and in all configurations. This negative trend continues on an increasing value of P/e, but the level of decrease is not as strong. It is worth noting that the P/e=10.71 set has the highest Nu_{imp} value of 3.28 at Re=6000 and P/e=17.86 set has the minimum improvement values.

Turbulence Characteristics

In Figures 8 and 9, the turbulent kinetic energy (TKE) and turbulent intensity (TI) profiles of the rib-roughened SAH at P/e=10.71 have been plotted with different Reynolds numbers. It is seen in the analysis that the highest intensities of turbulence are between the first and second ribs based on the highest contour values. Both TKE and TI show a progressive weakening of both streams in the direction of their streamwise. The contours indicate that there is increased turbulence in the close area of the ribs and the values decrease gradually as the distance increases away. These high TKE and TI maps are associated with regions of increased turbulent mixing and increased shear stress generation.

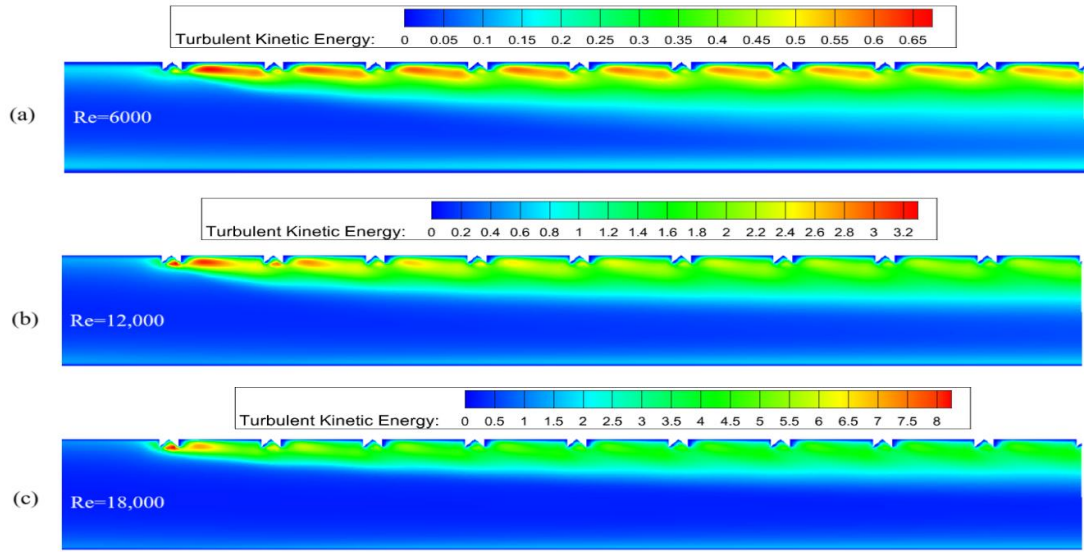

Figure 8. Contours of TKE with $P/e = 10.71$.

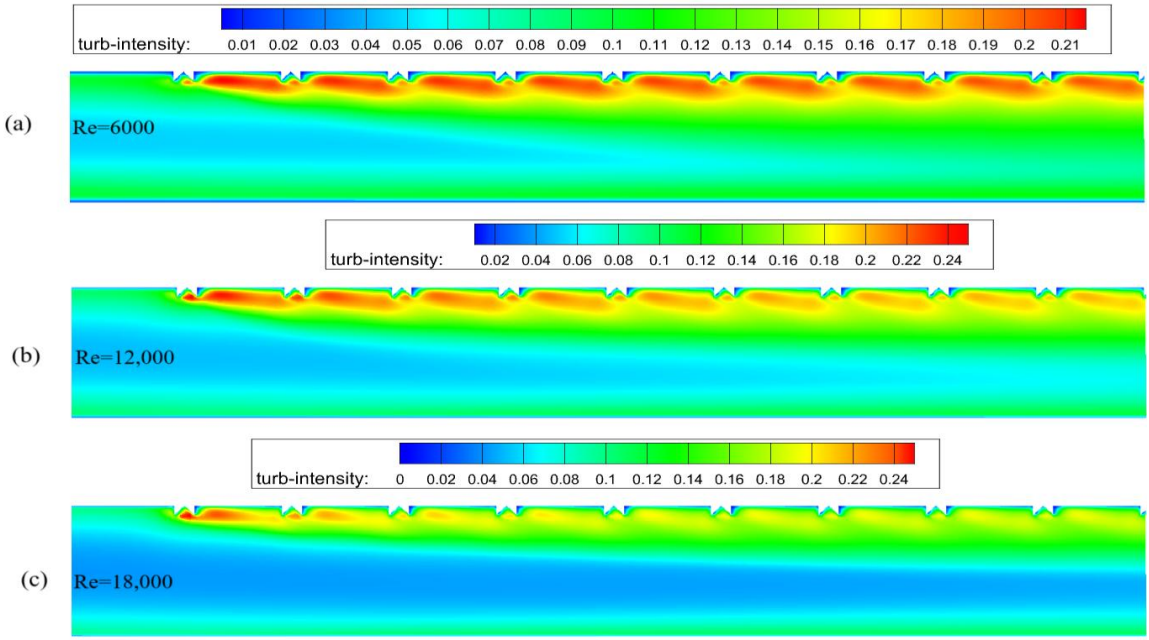

Figure 9. Contours of TI with $P/e = 10.71$.

The emerging flow properties cause shear stress dominance in the boundary layer that gradually changes to rib-induced turbulence as one heads further down the flow or towards the exit in the streamwise direction. Ribs increase the efficiency of eddy generation by impingement of high velocity airflow and W shaped ribs are especially good at increasing TKE and TI. The rib induced vortices in the vicinity of the collector plate and the high wall shear stress reinforce large momentum diffusion into the core flow, and consequently enhance thermal exchange of the heated surface. The TKE and TI curves affirm that, the higher the Reynolds number the greater the flow turbulence. This high level of turbulence allows the high level of cross-stream mixing, which leads to the successful entrains the cooler mainstream air into the inter-rib areas, and significantly enhances the heat transfer performance.

Velocity Contour

Figure 10 illustrates the velocity contours for various P/e ratios at Re= 12,000. As air moves through the rectangular duct, the ribs on the collector plate act like nozzles, accelerating the flow locally. Downstream, the increased velocity enhances turbulence, generating vortices near the rib edges, which allows for more efficient transmission of heat from the heated plate to the contact fluid. Minimizing P/e increases the rib density per unit length, disrupting smooth flow and raising flow resistance. This amplifies localized turbulence and disturbs the boundary layer more significantly, further enhancing thermal exchange. The contour plots reveal distinct vortices forming between the ribs, with closer rib spacing producing more such vortices. Consequently, the TKE and TI rise, boosting heat transfer performance.

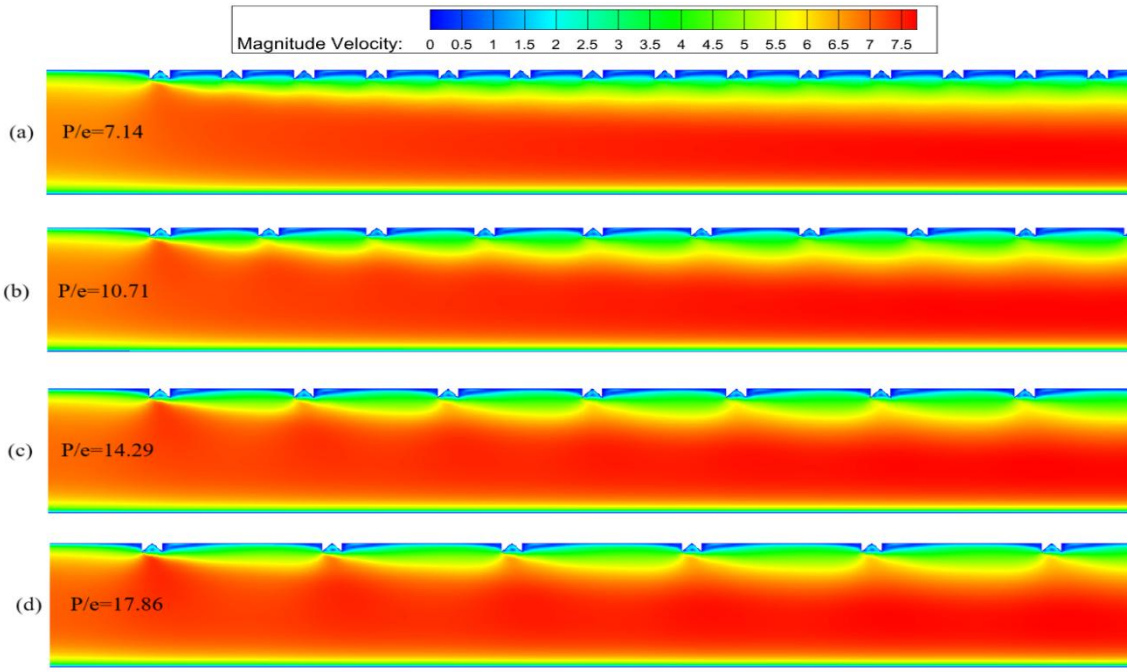

Figure 10. Velocity contours at $Re = 12{,}000$.

Streamlines

In the SAH channel, the ribs redirect airflow away from the plate wall at their junction. This abrupt expansion of the fluid creates a recirculation zone just downstream of each rib. The velocity streamline patterns in Figure 11 demonstrate this effect, displaying contours from a numerical simulation at Re=12,000 for different P/e ratios. Streamlines, which are imaginary lines indicating flow direction, typically reattach the channel's wall prior to the subsequent rib—except at P/e=7.14. This reattachment point, also called the impingement point, clarifies why the Nu rises initially with higher pitch ratios. Beyond this point, a fresh boundary layer starts forming, and the cycle of reattachment and recirculation repeats along the ribbed surface.The ribs induce vortices that locally enhance heat transfer, thus, the ribbed SAH is superior to its smooth-walled counterpart. Key mechanisms boosting heat transfer include boundary layer disruption due to flow separation, the reformation of the boundary layer, vortex generation, and increased turbulence-driven mixing near the ribs.

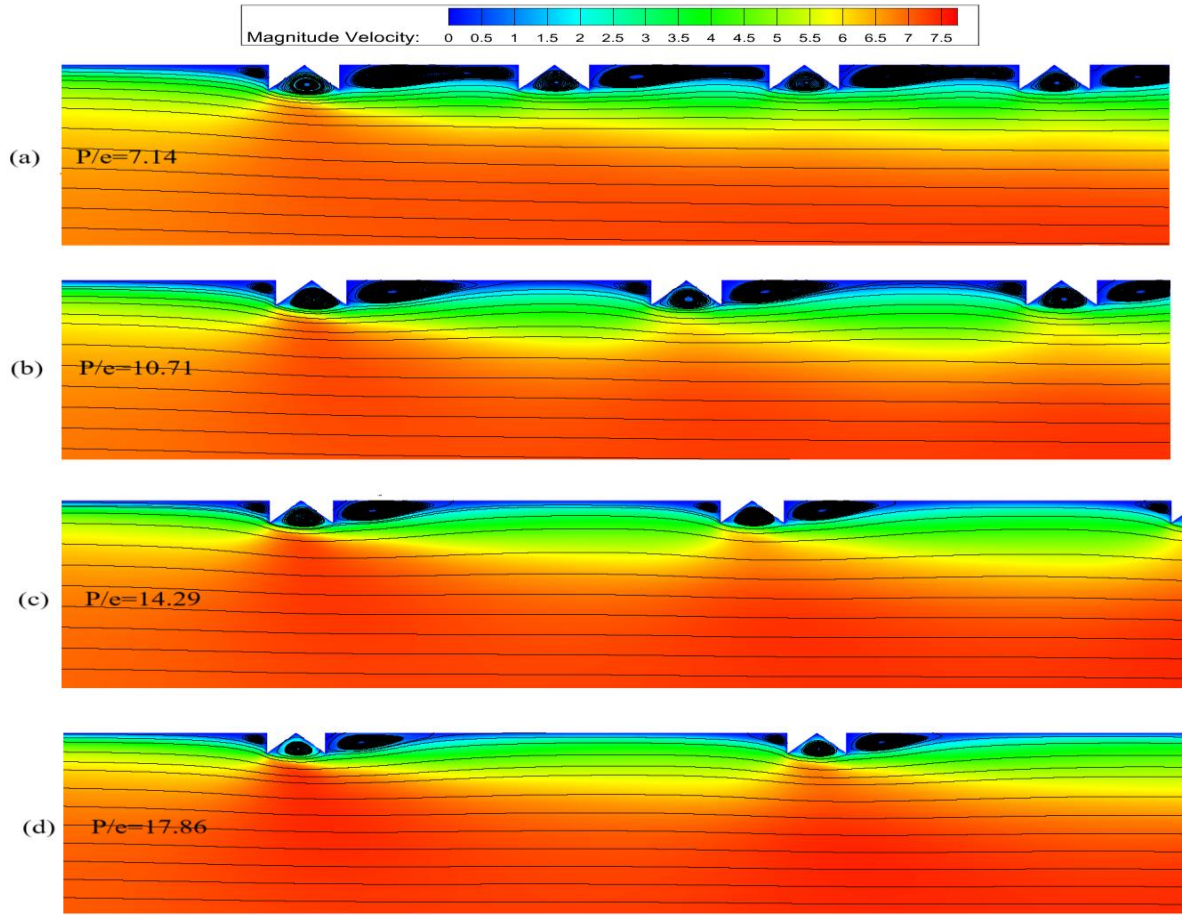

Figure 11. Streamlines formation close to W ribs at $Re = 12{,}000$.

Flow Analysis

Pressure drops are greater in ribbed SAHs compared to smooth ones due to the presence of artificial roughened, which improves thermal performance but increases frictional losses. In this part, the effect of two important non-dimensional factors on the behavior of the friction factor in ribbed SAH channels is examined: the P/e and Re

Average Friction Factor

Figure 12(a-b) shows how the average friction factor (f) is affected by Re and P/e. W-shaped ribs disturb the normal flow of the main stream inside the test section resulting in a great pressure drop. An increase in the flow blockage, turbulence and frictional resistance contribute to increasing the mean f of a ribbed duct in comparison with a smooth one. The findings proved the hypothesis that f diminishes with Re, which is explained by the change in the laminar flow to turbulent flow. And at larger Re the boundary layer is thinner and less stationary, having less of the effect of viscous sublayers. The increased mixing and momentum transfer in turbulent flow reduce the friction resistance to the flow, hence reducing friction factor. Of constant Re, average f is decreasing as P/e value increases. This has been explained by the fact that the number of ribs reduces with an increase in the P/e ratio. Fewer ribs result in reduced blockage of flow that consequently reduces the pressure drop and also reduces the mean f.

The data shown in Fig. 13 indicated how the ratio of the friction improvement (f_{imp}) changed with Re at different ratios of rib P/e. The ratio of the average f in a rib-roughened SAH to the smoothed-out one, f_{imp}, shows a steady increase with Re in all the experiments of the P/e configurations with the exception of P/e=17.86. There is a peak in the f_{imp} at P/e=7.14 that has a value of about 4.18 higher than the smooth channel baseline (Re=18,000). Minimal resistance to flow is observed at P/e=17.86, which proves the usefulness of increased rib spacing.

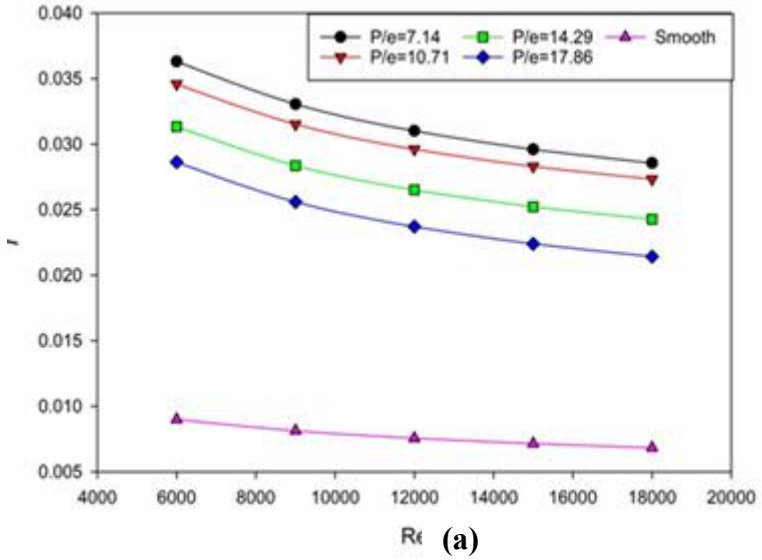

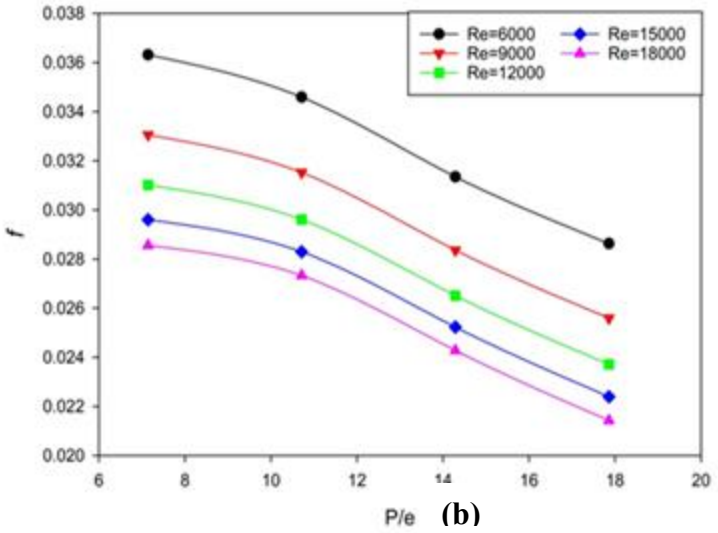

Figure 12. Average f verses (a) Re, (b) P/e

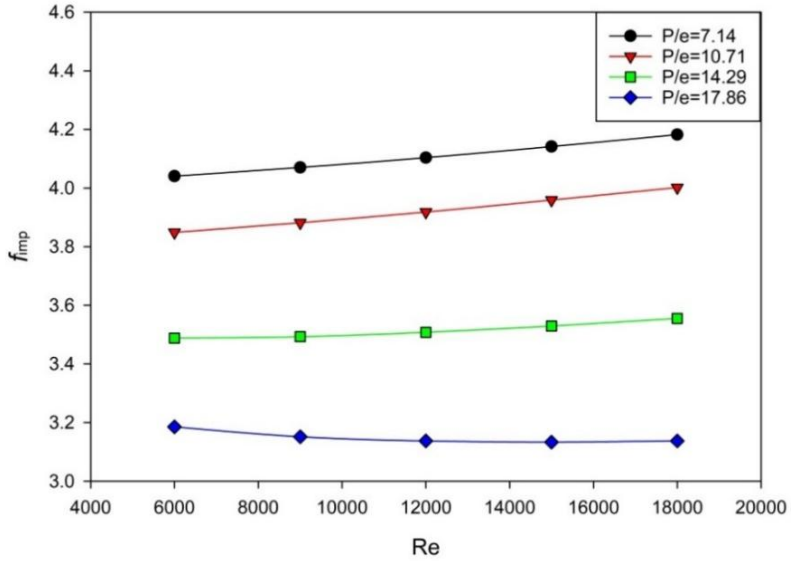

Figure 13. f_{imp} ratio verses Re at varying P/e values

Static Pressure Contours

Figure 14 illustrates the static pressure at the ribbed duct of different pitch configurations at Re = 12,000. The contours of pressure provide the important flow dynamics such as disruption of the W-shaped ribs in the test section. When the air enters the cavity, it causes the ribs to decelerate suddenly around the vertical rib face wherein high-pressure areas occur locally. The flow separation takes place beyond the rib tip resulting in the creation of a low-pressure recirculation region downstream. The pressure recovery occurs whereby the flow is reconnected to the absorber plate by the next ribs. Separation, recirculation and reattachment are the three phenomena that occur and result in great pressure losses. Also, the roughing surface contributes to acceleration of air, which then results in a sharp decrease in pressure between the duct inlet and outlet volume. Ribbed surfaces contribute to better thermal performance by increasing the heat transfer rate, however, the friction loss is also high, which requires the pumping power to sustain the airflow.

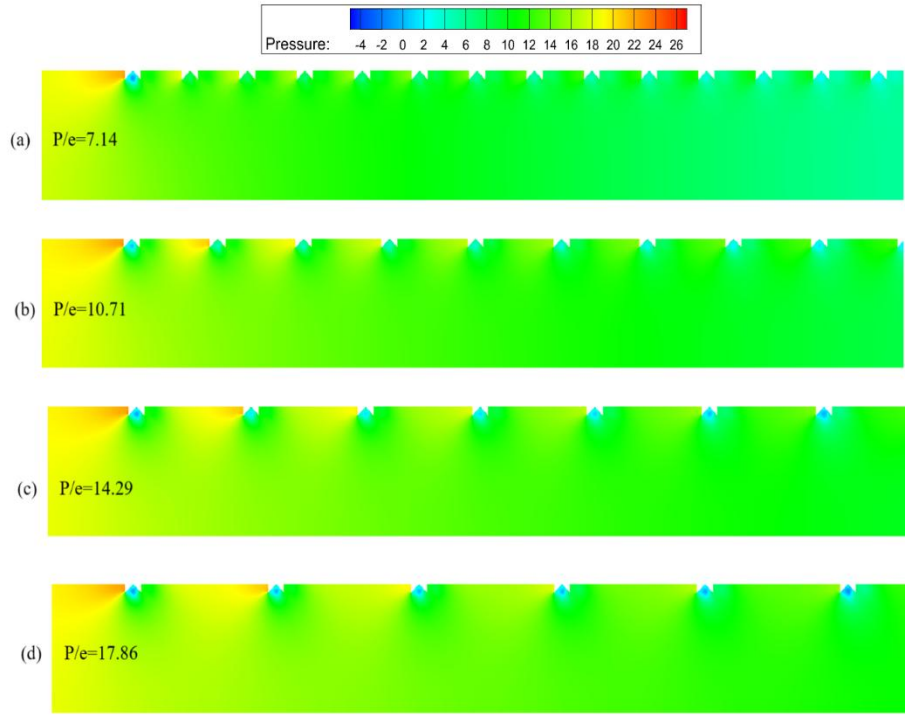

Figure 14. Pressure contours at $Re = 12{,}000$

Thermo-Hydraulic Performance Analysis

Thermal performance of a SAH is enhanced by roughening the surface of the absorber plate but it increases the pumping power requirements as a result of high power losses. Nevertheless, ribbed SAH designs are highly beneficial, and they are much more effective in terms of increasing the heat transfer rate with a relatively small increase in airflow resistance.

The f-Re-P/e relations demonstrate a critical compromise in design - reduction in P/e with smaller rib spacing, which improves the heat transfer in a turbulence-intense flow, costs more and more pumping power in disproportional amounts. One of the most important parameters of a SAH design is the choice of the geometric setting that will provide the best thermal characteristics and the minimal use of energy. In order to measure this balance, scholars use a thermo-hydraulic performance parameter (THPP), introduced by Webb and Eckert (Eq. 15). This is an overall measure that, quantitatively, measures the trade-off between the increase in heat transfer (measured by Nuimp) and increase in the flow resistance (measured by fimp). The THPP is efficient in balancing thermal improvement and the cost penalty of extra pumping power.

Figure 15 illustrates the dependence of the THPP on Re on various rib structures. The findings show that the value of THPP always has a value that is greater than unity, and has the value between 1.578 to 2.1 in all the conditions examined. An inverse behavior is found to be consistent between THPP and Re across all the rib geometries. With the W-rib configuration, the geometric parameters of P/e=10.17 maximum THPP occur at Re=6000. Through the

analysis of thermal-hydraulic performance (THPP), the current CFD results when compared against available high-performance data in Table 2 indicate that the optimized turbulator is much more efficient than the majority of the predecessors, which is reflected in the last column.

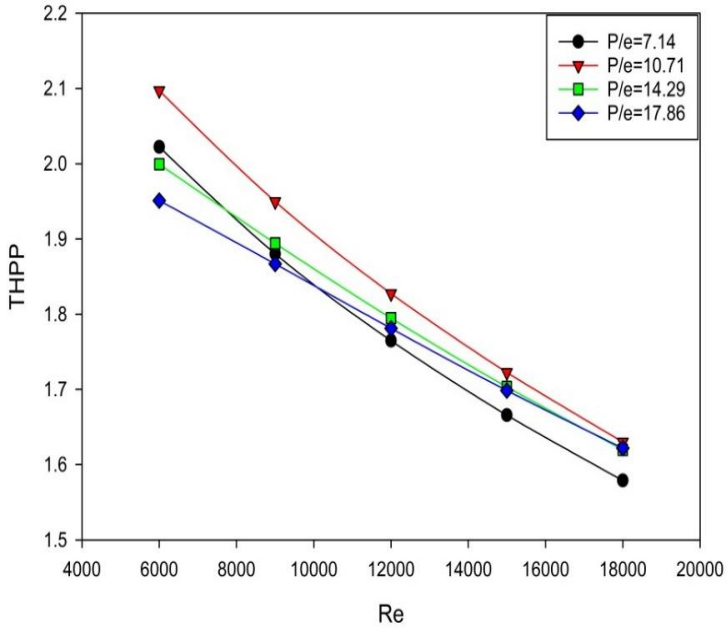

Figure 15. Variation of THPP with Re.

Table 2. A comparison of the present THPP findings with existing literature.

Turbulator types	Authors	$THPP_{max}$
Circular transverse wire rib	Bhagoria and Yadav (2013a)	1.65
Square sectioned rib	Bhagoria and Yadav (2014b)	1.88
Semicircular rib	Bhagoria and Yadav (2014c)	1.71
Reverse L-shaped ribs	Gawande et al. (2016b)	1.9
Quarter-circular	Mahananda and Senapati (2021)	1.88
B-shapes	Rautela et al. (2023)	1.47
W shaped ribs	Present	2.1

Conclusion

The numerical study is a two-dimensional model of computational domain to study the thermo-hydraulic performance of SAH duct with transverse W-shaped ribs. The paper systematically compares the effect of important dimensionless factors, - such as Re, P/e constancy e/D - on Nu and f. Concisely, the conclusions of the research are as follows:

1. It is shown that the ribbed SAH duct has a great improvement in the thermal performance compared to a plain duct SAH, where its Nu value is about 2.978 times higher in comparison with plain duct SAH at P/e = 10.71 and Re = 6000.
2. The f penalty is high with the value of 4.393 times the smooth duct at the P/e = 7.14 and Re = 18,000.
3. In the case of SAH with the suggested turbulator, the highest THPP was at Re=6000 with optimum geometric ratios of P/e = 10.17.
4. Flow field images (streamlines, pressure contours, turbulence parameters) were acquired of the W-rib configuration and were used to explain the thermo-fluid dynamic interactions of the system performance.

Scientific Ethics Declaration

* The authors declare that the scientific ethical and legal responsibility of this article published in EPSTEM journal belongs to the authors.

Conflict of Interest

* The authors declare that they have no conflicts of interest

Funding

*There is no funding

Acknowledgements or Notes

* This article was presented as a poster presentation at the International Conference on Engineering and Advanced Technology (ICEAT) held in Selangor, Malaysia on July 23-24, 2025.

References

Abbas Alhilali, H. A., Al-Chlaihawi, K., Zarzoor, A. K., & Flayyih, M. A. (2025). Optimization of thermohydraulic parameters in solar air heater ducts featuring I-shaped ribs. *Heat Transfer, 54*(6), 3790–3814.

Al-Chlaihawi, K. K. I., Alyas, B. H., & Badr, A. A. (2023). CFD based numerical performance assessment of a solar air heater duct roughened by transverse-trapezoidal sectioned ribs. *International Journal of Heat and Technology, 41*(5), 879–888.

Al-Chlaihawi, K., Alyas, B. H., & Abdullah, B. N. (2024). Optimizing of heat transfer and flow characteristics within a roughened solar air heater duct with compound turbulators. *Asia-Pacific Journal of Chemical Engineering, 19*(5), e3126.

Alrashidi, A., Altohamy, A. A., Abdelrahman, M. A., & Elsemary, I. M. M. (2024). Energy and exergy experimental analysis for innovative finned plate solar air heater. *Case Studies in Thermal Engineering, 59*, 104570.

American Society of Heating, Refrigerating and Air-Conditioning Engineers. (2003). *ANSI/ASHRAE Standard 93-2003: Methods of testing to determine the thermal performance of solar collectors*. ASHRAE.

Bhagoria, J. L., & Yadav, A.S. (2013b). Heat transfer and fluid flow analysis of solar air heater: A review of CFD approach. *Renewable and Sustainable Energy Reviews, 23*, 60–79.

Bhagoria, J. L., & Yadav, A.S. (2014b). A numerical investigation of square sectioned transverse rib roughened solar air heater. *International Journal of Thermal Sciences, 79*, 111–131.

Bhagoria, J. L., & Yadav, A.S. (2013a). A CFD based heat transfer and fluid flow analysis of a solar air heater provided with circular transverse wire rib roughness on the absorber plate. *Energy, 55*, 1127–1142.

Bhagoria, J. L., & Yadav, A.S. (2014a). A CFD based thermo-hydraulic performance analysis of an artificially roughened solar air heater having equilateral triangular sectioned rib roughness on the absorber plate. *International Journal of Heat and Mass Transfer, 70*, 1016–1039.

Bhagoria, J. L., & Yadav, A.S. (2014c). A numerical investigation of turbulent flows through an artificially roughened solar air heater. *Numerical Heat Transfer, Part A: Applications, 65*(7), 679–698.

Bopche, S. B., & Tandale, M. S. (2009). Experimental investigations on heat transfer and frictional characteristics of a turbulator roughened solar air heater duct. *International Journal of Heat and Mass Transfer, 52*(11–12), 2834–2848.

Chamoli, S., Lu, R., Xu, D., & Yu, P. (2018). Thermal performance improvement of a solar air heater fitted with winglet vortex generators. *Solar Energy, 159*, 966–983.

Chaube, A., Sahoo, P. K., & Solanki, S. C. (2006). Analysis of heat transfer augmentation and flow characteristics due to rib roughness over absorber plate of a solar air heater. *Renewable Energy, 31*(3), 317–331.

Fox, R. W., McDonald, A. T., & Pritchard, P. J. (1994). *Introduction to fluid mechanics* (4th ed.). John Wiley & Sons.

Gawande, V. B., Dhoble, A. S., Zodpe, D. B., & Chamoli, S. (2016a). Experimental and CFD-based thermal performance prediction of solar air heater provided with chamfered square rib as artificial roughness. *Journal of the Brazilian Society of Mechanical Sciences and Engineering, 38*(3), 643–663.

Gawande, V. B., Dhoble, A. S., Zodpe, D. B., & Chamoli, S. (2016b). Experimental and CFD investigation of convection heat transfer in solar air heater with reverse L-shaped ribs. *Solar Energy, 131*, 275–295.

Gupta, D., Solanki, S. C., & Saini, J. S. (1993). Heat and fluid flow in rectangular solar air heater ducts having transverse rib roughness on absorber plates. *Solar Energy, 51*(1), 31–37.

Kakaç, S., Yener, Y., & Pramuanjaroenkij, A. (2013). *Convective heat transfer* (3rd ed.). CRC Press.

Karwa, R. (2003). Experimental studies of augmented heat transfer and friction in asymmetrically heated rectangular ducts with ribs on the heated wall in transverse, inclined, V-continuous and V-discrete pattern. *International Communications in Heat and Mass Transfer, 30*(2), 241–250.

Kumar, A., Saini, R. P., & Saini, J. S. (2014). A review of thermohydraulic performance of artificially roughened solar air heaters. *Renewable and Sustainable Energy Reviews, 37*, 100–122.

Launder, B. E., & Spalding, D. B. (1972). *Lectures in mathematical models of turbulence*. Academic Press.

Layek, A., Saini, J. S., & Solanki, S. C. (2009). Effect of chamfering on heat transfer and friction characteristics of solar air heater having absorber plate roughened with compound turbulators. *Renewable Energy, 34*(5), 1292–1298.

Mahanand, Y., & Senapati, J. R. (2021). Thermo-hydraulic performance analysis of a solar air heater (SAH) with quarter-circular ribs on the absorber plate: A comparative study. *International Journal of Thermal Sciences, 161*, 106747.

Olfian, H., Zabihi Sheshpoli, A., & Mousavi Ajarostaghi, S. S. (2020). Numerical evaluation of the thermal performance of a solar air heater equipped with two different types of baffles. *Heat Transfer, 49*(3), 1149–1169.

Patel, Y. M., Jain, S. V., & Lakhera, V. J. (2020). Thermo-hydraulic performance analysis of a solar air heater roughened with reverse NACA profile ribs. *Applied Thermal Engineering, 170*, 114940.

Patel, Y. M., Jain, S. V., & Lakhera, V. J. (2021). Thermo-hydraulic performance analysis of a solar air heater roughened with discrete reverse NACA profile ribs. *International Journal of Thermal Sciences, 167*, 107026.

Prasad, K., & Mullick, S. C. (1983). Heat transfer characteristics of a solar air heater used for drying purposes. *Applied Energy, 13*(2), 83–93.

Rautela, M., Sharma, S. L., Bisht, V. S., Debbarma, A., & Bahuguna, R. (2023). Numerical analysis of solar air heater roughened with B-shape and D-shape roughness geometry. *Journal of Heat and Mass Transfer Research, 10*(1), 101–120.

Roy, B., Reddy, D. S., & Khan, M. K. (2024). Performance investigation of a solar air heater artificially roughened with Joukowski airfoil ribs. *Journal of Solar Energy Engineering, 146*(1), 011004.

Sahu, M. K., Sharma, M., Matheswaran, M., & Maitra, K. (2019). On the use of longitudinal fins to enhance the performance in rectangular duct of solar air heaters—A review. *Journal of Solar Energy Engineering, 141*(3), 030802.

Sharma, S. L., Kishor, K., Bisht, V. S., Debbarma, A., & Gaur, A. (2024). CFD analysis of artificially roughened solar air heater: A comparative study of C-shape, reverse C-shape, and reverse R-shape roughness element. *International Journal of Ambient Energy, 45*(1), 2331240.

Sharma, S., Das, R. K., & Kulkarni, K. (2021). Performance evaluation of solar air heater using sine wave shape obstacle. In S. K. Acharya & D. P. Mishra (Eds.), *Current advances in mechanical engineering* (pp. 541–553). Springer.

Verma, S. K., & Prasad, B. N. (2000). Investigation for the optimal thermohydraulic performance of artificially roughened solar air heaters. *Renewable Energy, 20*(1), 19–36.

Webb, R. L., & Eckert, E. R. G. (1972). Application of rough surfaces to heat exchanger design. *International Journal of Heat and Mass Transfer, 15*(9), 1647–1658.

Yadav, S., & Saini, R. P. (2020). Numerical investigation on the performance of a solar air heater using jet impingement with absorber plate. *Solar Energy, 208*, 236–248.

Author(s) Information

Kadhim Al-Chlaihawi
University of Al-Qadisiyah, Department of Mechanical Engineering, , Al Diwaniyah, Al-Qadisiyah, 58001, Iraq
Contact e-mail: *kadhim.idan@qu.edu.iq*

Sarah Ahed Mohammed Al-Hasnawi
Al-Furat Al-Awsat Technical University, Department of Electrical Engineering Technologies, Al-Musayyab 51006, Babil, Iraq.

Ahmed Kadhim Zarzoor
University of Al-Qadisiyah, Department of Mechanical Engineering,, Al Diwaniyah, Al-Qadisiyah, 58001, Iraq

To cite this article:

Al-Chlaihawi, K., Al-Hasnawi, S.A.M., & Zarzoor, A.K. (2025). Numerical investigation of thermal - hydraulic performance of a solar air heater duct with transverse W-shaped rib turbulators. *The Eurasia Proceedings of Science, Technology, Engineering and Mathematics (EPSTEM), 37,* 255-271.